

Post-flare loops of May 16, 1981

Spectral analysis

Xiao-Ma Gu^{1,2}, You-Ji Ding², Zhi Luo², and Brigitte Schmieder³

¹ CCAST (World Laboratory), P.O. Box 8730, Beijing, 100080

² Yunnan Observatory, P.O. Box 110, Kunming, YN 650011, China

³ Observatoire de Paris- Meudon, DASOP, URA 2080, F-92195 Meudon Principal Cedex, France

Received 24 September 1996 / Accepted 21 November 1996

Abstract. We present the analysis of $H\alpha$ spectra obtained during a two-ribbon flare observed on the solar disk on May 16, 1981 at Yunnan Observatory with the Spectra-Spectroheliograph (SSHG). The complicated asymmetric profiles produced by the post-flare loops overlying flare ribbons are analysed with a fast method based on the cloud model method. This method takes into account the bright background of the loops and allows computation of the physical quantities of loops crossed by the slit: velocity field, optical thickness, source function and Doppler width. Using the scanning spectra of the region, we obtain 2-D maps of these parameters. The validity of the method used is compared with other methods and the sensitivity of parameters to solution is discussed in details. The results obtained with this method are compared with those given by Heinzel et al. (1992) using a fully non-LTE approach.

Key words: Sun: flares – methods: data analysis

1. Introduction

Post-flare loops are frequently observed at the limb in $H\alpha$ and more recently in X-rays due to the new generation of space instrumentation (see reviews of Švestka 1989, and Schmieder 1992). Already with Skylab, X-ray post-flare loops were observed (Cheng 1980), then with SMM (Švestka et al. 1987) and with Yohkoh (Tsuneta 1996 a, b and references therein, Schmieder et al. 1995, 1996). A crucial problem is the formation of post-flare loops. A common explanation is the reconnection of the magnetic field lines after a large flare (Forbes and Malherbe 1986, Forbes and Acton 1996). Several observations are in favour of this explanation. In HXT/Yohkoh images the cusp due reconnection is often observed in hard X-ray (Masuda 1994) and below it X-ray loops are observed with Yohkoh/SXT. Associated $H\alpha$ loops are generally observed by ground-based

observatories. Schmieder et al. (1996) have shown that this scenario is plausible in one studied case where a long set of data in multi-wavelengths was performed, during Yohkoh campaign. But Feldman and Seely (1995) going back to Skylab data argue against this possibility.

In the interpretation of cool loops being due to cooling of the hot loops formed during the reconnection process by conduction and radiative losses, it is important to have the value of the electron density of both hot and cool loops. The estimation of the electron density of cool loops require spectra and interpretation of the profiles of the lines by a non-LTE radiative transfer treatment. First of all, only a few spectral data are available: we can quote the spectra obtained with the Multi-Channel Subtractive Double Pass (MSDP) spectrograph for the post flare loops of May 16, 1981 and May 5, 1989 (Heinzel et al. 1992, Gu et al. 1992). Here we use data of the Yunnan observatory Spectra-Spectroheliograph (SSHG) which has a better spectral resolution than the MSDP and larger wavelength range but a lower spatial resolution. We will present a method of cloud models to interpret the $H\alpha$ profiles observed on the disk based on the existence of 2 layers and compare with previous results obtained with other methods analysing MSDP observations of the same event. We will show that this method is quite powerful and fast compared to full radiative transfer treatment but has some limits.

2. Instruments and observations

We analyse $H\alpha$ spectra obtained at Yunnan Observatory with the SSHG mounted on a telescope of an aperture of 300 mm. The diameter of the Sun is 152 mm in the slit plane. The active region was scanned with a step of 4 arc sec. It takes two or three minutes to scan an active region. The flare patrol telescope equipped by an $H\alpha$ filter gave a good survey of the flare. The flare occurs in the AR 3106 located on the 16th May 1981 on the disk (N11, E14). It is a two-ribbon flare of class IX/3B beginning at 08:14 UT, with a maximum at 08:47 UT and ending at 09:38 UT. A large post-flare loop system developed during that time

Send offprint requests to: Xiaoma-Gu

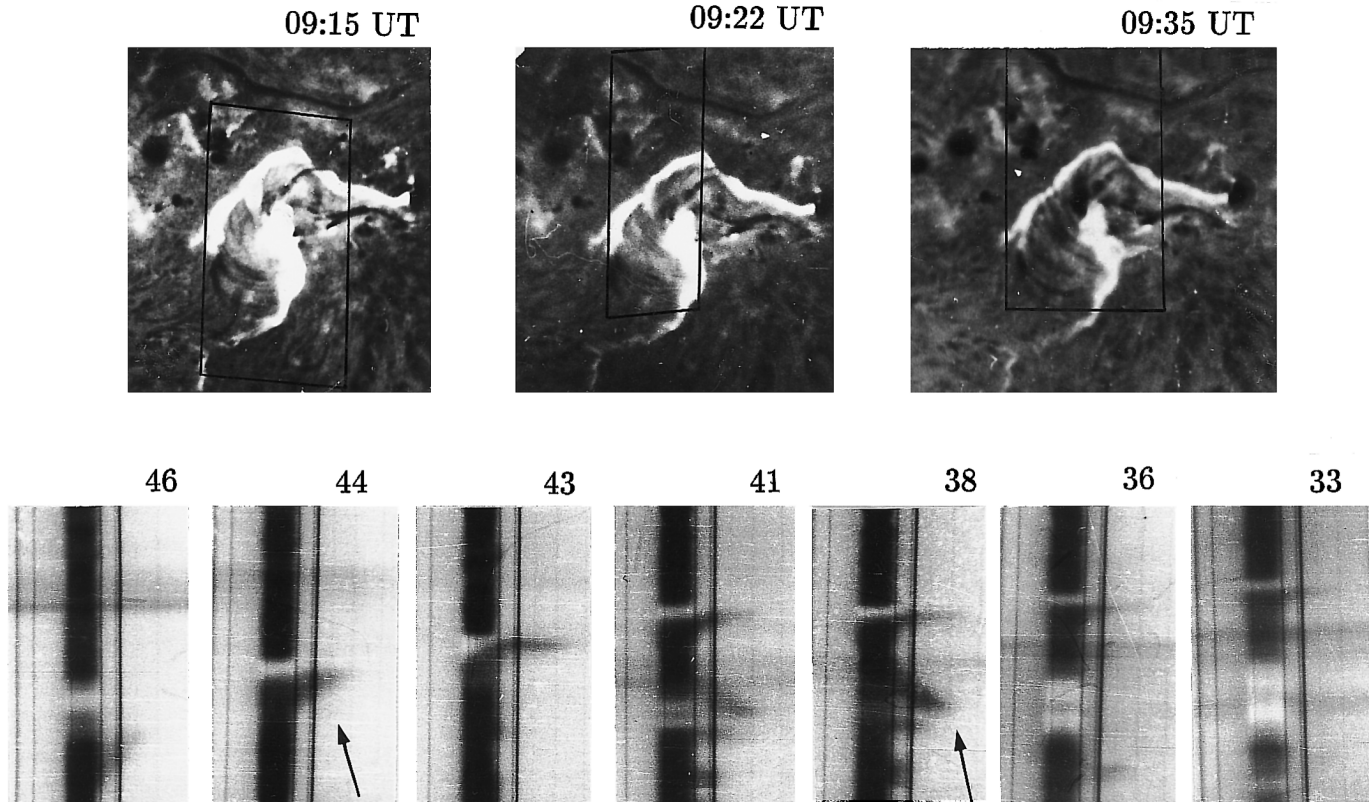


Fig. 1. Flare of May 16, 1981 observed at Yunnan observatory **a** with the $H\alpha$ filtergraph, **b** with the Spectrograph SSHG. The spectra correspond to positions of the slit in the box in the central image of 09:22 UT. The numbers are the number of the scan. The bright upper part in the $H\alpha$ line is the long thin upper bright ribbon (northern) the low thick bright part correspond to the thick southern ribbon. Note the large velocities of the loops indicated by arrows

(Fig. 1a). This flare has been extensively studied already with the MSDP of Meudon Observatory (Schmieder et al., 1987, 1990, Heinzel et al. 1992), and preliminary results obtained with the SSHG were presented by Luo (1987). The main point focus in Schmieder's papers was the study of chromospheric ablation in the ribbons due to heat conduction propagation. In Heinzel et al. (1992), the $H\alpha$ profiles of the post-flare loops observed with the MSDP were analysed by using the classical cloud-model method to estimate the source function S of the loops and the value of S was used in NLTE models to derive the pressure and the electron density. Due to the lower spectral resolution of the MSDP (0.3 \AA), the computation could be achieved only in a few points in the loops.

The post-flare loops of the event of May 16, 1981 were scanned in Yunnan at three different times around 09:15, 09:22, 09:33 UT in an area represented by a box in the Fig. 1a. Around 60 scans are available for each time. The Fig. 1b displays some of them corresponding to the central picture of Fig. 1a at 09:22 UT. The brightest parts of the $H\alpha$ line correspond to the ribbons (northern and southern ones). The dark parts of the line with large redshifts represent the high doppler shifts of the matter in the post-flare loops. We propose in this paper a new method to analyse the spectra.

3. Method of spectral analysis

In the classical cloud model method (Beckers 1964), the contrast of $H\alpha$ is computed from the difference of the observed intensity at each pixel and a mean profile intensity computed over the quiet chromosphere. It has been shown that this method is not the best for the case of post-flare loops because they are generally lying over bright and inhomogeneous region (Gu et al. 1992). Another method was proposed by Mein and Mein (1989) called first-order differential cloud-model method (DCM1) which takes into account the background intensity below the loops. Here we use another technique using the quiet-Sun profile as background (see Gu et al. 1992). The contrast profiles have two components, one positive and one negative as it is visible in the spectra that we have observed (Fig. 2). So we assume that the observed radiation is the result of transfer of chromospheric radiation through two clouds, one corresponding to a brighter region than the quiet Sun and the other to the loop itself. These two layers have different physical conditions (source function, optical thickness, velocity, Doppler width). This method has been applied to $H\alpha$ profiles of the MSDP spectrograph (Gu et al. 1992). Assuming constant source functions S_1 and S_2 in the two clouds, we write the contrast profile (C_λ):

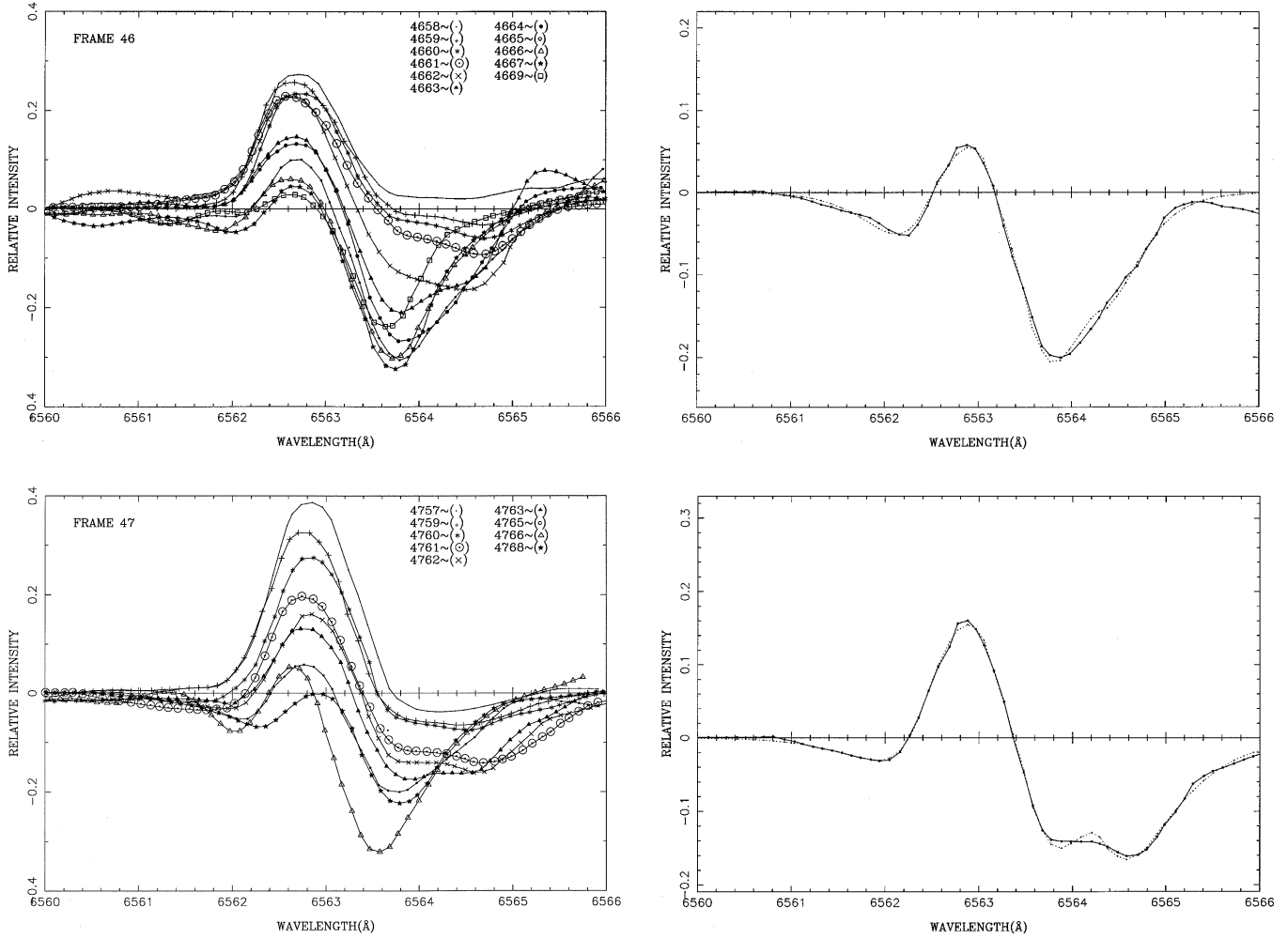


Fig. 2. (left panels) Contrast profiles along the slit for scans 46 and 47. The numbers are the positions of pixels along the slit (right panels) Example of observed contrast profiles n° 4765 (top) and n° 4762 (bottom) (solid line) and the fitted contrast profiles (dotted line).

$$C_{\lambda} = \frac{I(\lambda) - I_0(\lambda)}{I_0(\lambda)}$$

with I_0 the radiation incident on the bright cloud from below and $I(\lambda)$ the emergent radiation after crossing the two clouds.

$$I(\lambda) = I_0(\lambda)e^{-(\tau_1 + \tau_2)} + S_1(1 - e^{-\tau_1})e^{-\tau_2} + S_2(1 - e^{-\tau_2})$$

where τ_1 and τ_2 are given by the following equations where $j=1$ is the bright background and 2 the post-flare loops:

$$\tau_j = \tau_{0,j} e^{-\left(\frac{\Delta\lambda - \Delta\lambda_j}{W_j}\right)^2}$$

and where τ_j , $\tau_{0,j}$ are the optical thickness respectively at $\Delta\lambda$ and in the line center; $\Delta\lambda_j$ and W_j ($\Delta\lambda_D$ in the Tables) are the Doppler shift and the Doppler width of the line of the j^{th} cloud respectively and $\Delta\lambda_j = \lambda_0 v_{c,j} / c$ where $v_{c,j}$ is the line of sight velocity of the j^{th} cloud ($j=1,2$).

We have applied this method to the spectra of SSHG. We take reasonable values of the parameters as initial conditions

(see next section). We fit the observational profiles with the theoretical ones by using the least-square method developed by Fang (1985), see Appendix. The accuracy of the mathematical fitting is good and the solution converges rapidly (Fig. 2).

4. Validity of the method

In the Fig. 2 are displayed the profile contrasts of pixels along the slit crossing successively a bright region and the post-flare loops. We see that the shape of the contrast changes progressively from emission to absorption. We have tested the accuracy of the results for 2 profiles, one concerning mainly a bright portion, the other one the loop. The initial values are estimated approximately. For example, as $\Delta\lambda_D \sim 0.3-0.5 \text{ \AA}$ corresponds to a microturbulence of 10 km s^{-1} , we choose $\Delta\lambda_D = 0.5 \text{ \AA}$; $\Delta\lambda_0$ equal to the displacement of the center of the contrast profile, $\tau_{0,1}$ and $\tau_{0,2}$ equal to 0.5 or 1 according to the relative importance of the absorption and the emission part in the contrast profiles, S lower than 1 (in unit = % I_{cont}), I_{cont} being the continuum intensity. They are derived for the different pixels

Table 1. Comparison of different results obtained with different initial parameters for the flare of May 16, 1981

Parameters	$\tau_{0,1}$	$\tau_{0,2}$	$\Delta\lambda_{D,1}(\text{\AA})$	$\Delta\lambda_{D,2}(\text{\AA})$	$\Delta\lambda_{0,1}(\text{\AA})$	$\Delta\lambda_{0,2}(\text{\AA})$	S_1	S_2
Initial values	0.350	0.996	1.080	0.593	0.371	0.781	0.100	0.360
Fitting results	0.3478	0.9976	1.0797	0.5935	0.3720	0.7806	0.0997	0.3596
$\tau_{0,1,0} +10$	+5.75	+0.08	-0.90	-0.76	+1.45	-0.18	+7.23	+0.74
$\tau_{0,1,0} +20$	+11.80	+0.025	-1.93	-1.62	+3.20	-0.16	+14.34	+1.47
$\tau_{0,1,0} -50$	-24.49	+3.04	+4.82	+3.69	-8.77	-1.31	-54.70	-2.38
$\tau_{0,2,0} +10$	-1.15	+9.40	-0.16	-1.84	-0.69	-0.20	-7.38	+1.29
$\tau_{0,2,0} +20$	-1.77	+18.83	-0.30	-3.75	-1.19	-0.24	-12.77	+2.39
$\tau_{0,2,0} -50$	-0.55	-0.13	+0.14	+0.05	-0.35	+0.05	-0.63	-0.04
$\Delta\lambda_{D,1,0} +10$	-14.21	+2.14	+3.71	+0.55	-3.37	-0.21	-21.72	-1.41
$\Delta\lambda_{D,1,0} +20$	-26.68	+4.15	+6.42	+2.54	-8.73	-0.88	-54.43	-2.57
$\Delta\lambda_{D,1,0} -50$	-23.04	+6.63	+3.59	+3.07	-10.17	-0.99	-55.12	-1.54
$\Delta\lambda_{D,2,0} +10$	-1.00	-0.45	-0.57	+6.30	-1.70	-0.81	-3.80	-0.05
$\Delta\lambda_{D,2,0} +20$	-2.62	-0.94	-1.28	+12.60	-3.79	-1.87	-8.92	-0.38
$\Delta\lambda_{D,2,0} -50$	-0.07	+3.39	+0.44	-1.85	+0.03	+0.66	+2.33	+0.53
$\Delta\lambda_{0,1,0} +10$	+1.08	+0.01	+0.19	-1.06	+6.15	-0.84	-4.28	+0.71
$\Delta\lambda_{0,1,0} +20$	+1.14	+0.89	+0.34	-1.00	+5.67	-1.78	-7.85	+0.81
$\Delta\lambda_{0,1,0} -50$	-25.34	+5.77	+4.25	+3.64	-11.30	-1.06	-59.62	-2.01
$\Delta\lambda_{0,2,0} +10$	-1.41	+0.64	+0.47	-1.12	-4.08	+2.29	+9.61	-0.41
$\Delta\lambda_{0,2,0} +20$	-2.83	+1.16	+0.73	-0.78	-4.29	+1.82	+5.78	-0.49
$\Delta\lambda_{0,2,0} -50$	-10.74	+3.77	+1.37	+1.87	+0.68	-2.71	-38.96	-0.01
$S_{1,0} +10$	+0.41	+0.05	+0.10	-0.25	-0.27	+0.19	+3.63	-0.10
$S_{1,0} +20$	+0.67	+0.13	+0.19	-0.55	-0.54	+0.43	+5.16	-0.06
$S_{1,0} -50$	-5.70	+1.41	+0.44	+1.54	+0.07	-1.56	-21.42	+0.00
$S_{2,0} +10$	-0.06	+0.69	-0.22	+0.12	+0.25	-0.16	-3.56	+0.33
$S_{2,0} +20$	-0.37	+2.25	-0.73	+1.54	-0.98	+0.01	-7.86	+0.89
$S_{2,0} -20$	-2.87	+1.06	+0.18	+1.03	-1.90	-0.63	-7.10	-0.24

Profile Number 4768. Subscript 1 is for flare ribbons and subscript 2 is for loops. Subscripts with “0” in the first column refer to an initial value. The unit of the data above is in percent (%), where “+” indicates an increase and “-” a decrease.

Table 2. Fitting results obtained with the ‘two-cloud model’ and the ‘one-cloud model’ methods for the flare of May 16, 1981

Parameters	$\tau_{0,1}$	$\tau_{0,2}$	W_1	W_2	$V_{c,1}$	$V_{c,2}$	S_1	S_2
Profile numbers	unit		\AA	\AA	km s^{-1}	km s^{-1}	$I_{cont.}$	$I_{cont.}$
4757	0.808	0.442	0.913	0.518	16.78	56.73	0.995	0.412
4759	0.846	0.391	0.867	1.002	4.80	45.80	0.846	0.413
4760	1.075	0.273	0.983	0.989	16.18	58.47	0.690	0.394
4761	0.628	0.688	1.268	1.235	-7.61	55.40	0.635	0.434
4762	0.702	0.878	1.478	0.910	37.35	45.67	0.544	0.457
4763	1.013	0.213	0.881	1.175	15.77	50.88	0.747	0.248
4765	0.537	0.953	1.113	0.671	23.95	39.22	0.292	0.413
4766	1.418	1.693	0.923	0.290	28.98	50.19	0.301	0.332
4768	0.348	0.998	1.080	0.594	17.00	35.70	0.100	0.360
4658	0.731		0.806		0.00		0.761	
4659	0.945		0.716		-2.48		0.687	
4660	0.676	0.356	0.699	0.775	-4.28	63.14	0.606	0.430
4661	0.477	0.449	0.756	0.784	-10.67	61.24	0.745	0.359
4662	0.438	0.746	0.647	0.789	-7.83	54.00	0.799	0.245
4663	0.309	1.085	0.544	0.747	-8.24	38.97	0.763	0.198
4664	0.296	2.043	1.093	0.667	-5.04	41.18	0.782	0.345
4665		1.397		0.584		48.73		0.286
4666		0.934		0.524		42.10		0.172
4667		0.689		0.508		40.50		0.014
4669		0.630		0.460		35.75		0.131

Subscript “1” indicates flare ribbons while subscript “2” indicates loops.

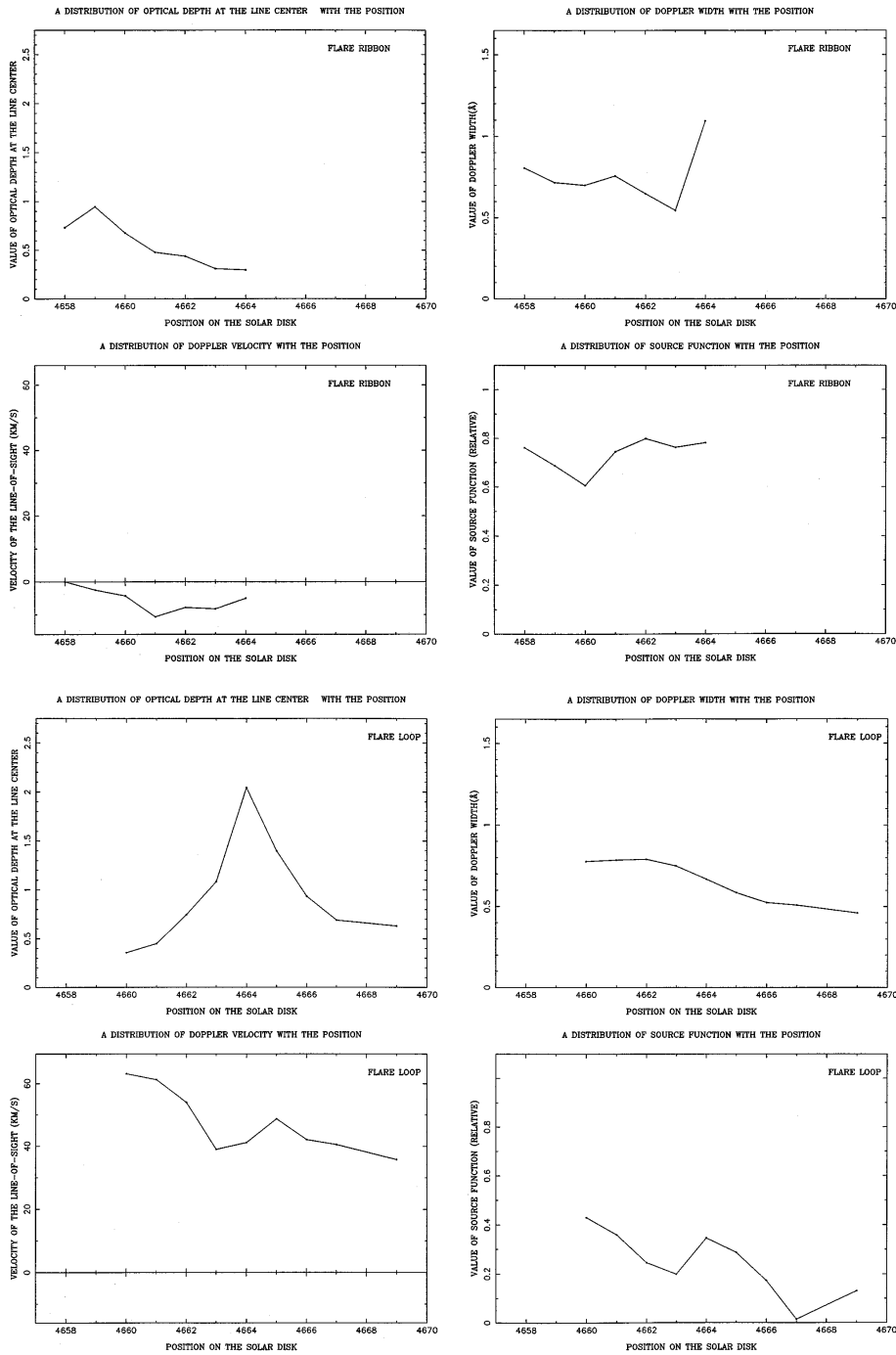


Fig. 3. Variation of the physical parameters S , τ , $\Delta\lambda$, $\Delta\lambda_D$ along the slit for scan 46. The loops are present in positions $x > 4663$ and $x > 4763$, respectively.

along the slit by continuity. Table 1 presents the initial values of the 8 parameters and their variation if we change their values one by one by an increase of 10%, 20% and even 50%. We see that the change of $\Delta\lambda_{0,2}$ is less than 1% for the loop, and $\Delta\lambda_{0,1}$ can reach 10%. The variation of the source function is less than 2.5% for the loop and reaches 5% for the cloud 1. For the loop the errors are not significant, for the cloud 1 the error can be of the same order as the variation of the initial conditions, i.e. for τ . We can conclude that this method is relatively accurate for the 4 parameters (S , τ_0 , $\Delta\lambda_D$ or W , and $\Delta\lambda_0$) concerning the loop. They are reasonable parameters with the same limits as

already exists for the classical cloud model method. The four parameters of a solution are not independent. When one parameter is large enough compared to a mean value, its determination is relatively accurate, that is the case for the cloud 2 velocity. For the bright background we should use the parameters with caution. S and τ for example are related to each other. It has been shown that the use of a constant source function in a cloud leads to some errors on the optical thickness and velocity (Mein et al. 1996).

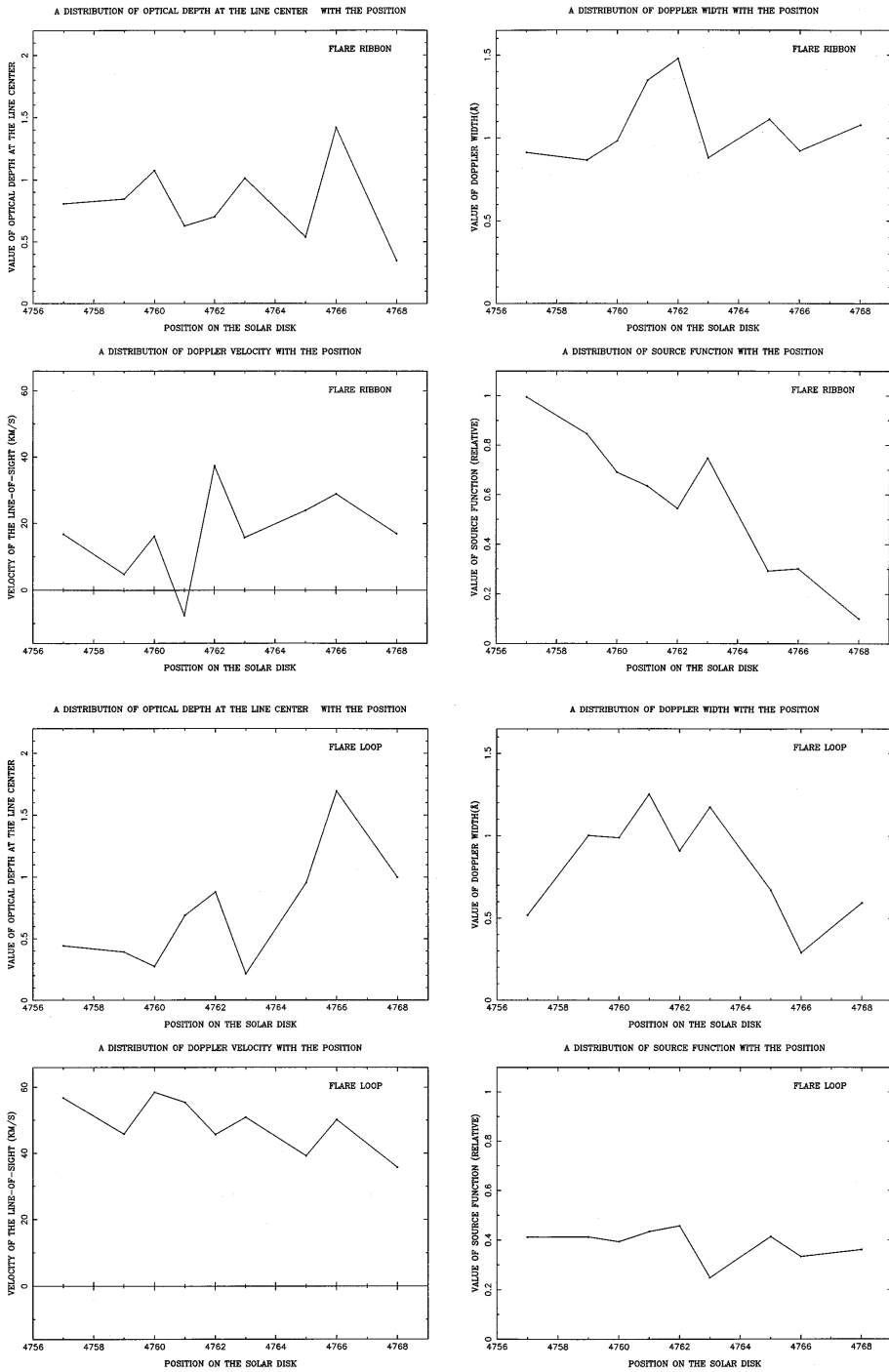


Fig. 4. Variation of the physical parameters S , τ , $\Delta\lambda$, $\Delta\lambda_D$ along the slit for scan 47. The loops are present in positions $x > 4663$ and $x > 4763$, respectively.

5. Physical parameters of the loop and the bright background

The results of scans 46 and 47 are presented in Table 2. For the loops the values τ_2 are close to 1 and S_2 around 0.36. We use the classical method when the contrast profile is simple with only one absorbing minimum. We have chosen the scans 46 and 47 because they correspond to points that have been already computed by using the DCM1 method applied to MSDP observations (Heinzl et al. 1992). The ribbons are present for value < 4664 and < 4763 respectively for the 2 scans 46 and 47. The

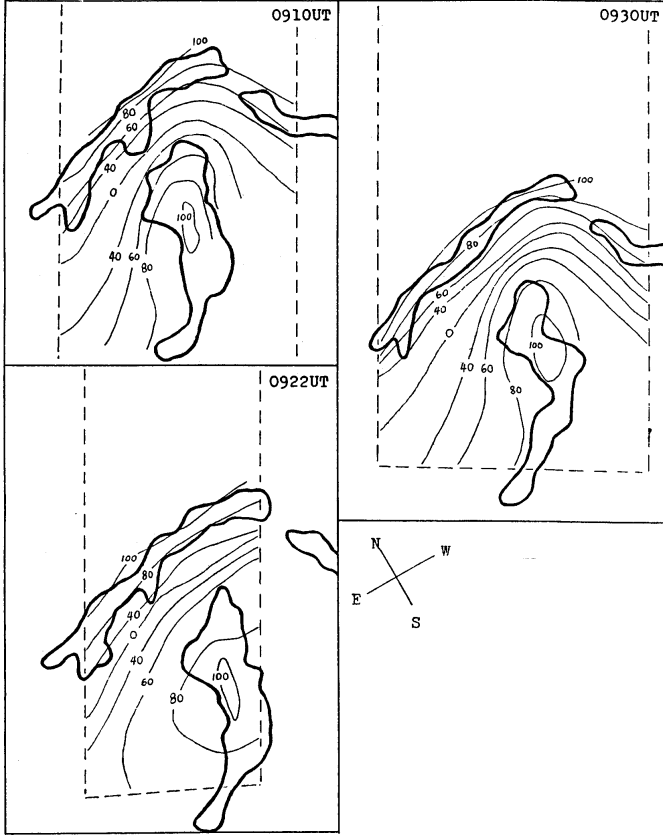
comparison with DCM1 results can be achieved with the scan 46 (profiles 63-69) and the scan 47 (62-68) and is presented in Table 3.

These results are in relatively good agreement, principally for the computations of the Doppler shifts of the loops. The results concerning the variation of the 8 parameters along the slit are displayed in Figs. 3, 4.

For the ribbons (cloud 1), the 4 parameters are related to each other because none of them are far from their mean value.

Table 3. Comparison of methods for the determination of the loop parameters (1 cloud, 2 clouds and DCM1)

parameter	SSHG/1 cloud	SSHG/2 clouds	MSDP/DCM1
S	13-38%	24-41%	17-34%
v	50- 40 km s ⁻¹	50-40 km s ⁻¹	40 km s ⁻¹
τ	0.6-2.6	0.3-2.3	$\delta\tau = 0.5-1.3$
W	1-0.5 Å		0.5-0.7 Å

**Fig. 5.** 2-D Isocontours of the magnitude of the velocity field (in km s⁻¹) overlaid on H α intensity maps of three different sets of flare ribbons with connecting post-flare loops.

In fact the ribbon profiles have to be analysed with a completely non-LTE treatment for a semi-infinite medium to get an accurate determination of the parameters.

On the other hand, the method is powerful for the analysis of the loop and gives good approximations of the loop parameters and can be compared to DCM1 method. This method is fast and can be applied to all the points of the different scans and 2-D maps that have been reconstructed. They are presented in Fig. 5 for the loops. We see large velocities near the ribbons where the loops are anchored. That is in agreement with the velocities of the matter flowing along post-flare loops (Wiik et al. 1996).

6. Electron density and gas pressure of the loops

We used approximations of non-LTE computation to derive other physical quantities (Table 4). From N_{O_2} , the column den-

sity of hydrogen atoms at the second level, we derived the electron density n_e in the loop and the gas pressure of electrons according to the following equation:

$$n_e \sim 3.2 \times 10^8 \sqrt{n_{O_2}} \text{ (Poland et al. 1971) with } N_{O_2} = n_{O_2} \times D.$$

This was derived for low density and static plasma. More generally it was confirmed in a NLTE prominence study by Heinzel et al. (1994). If the thickness D of the loops is assumed to be around 2000 km, $n_e \sim 2.5-5.6 \times 10^{10} \text{ cm}^{-3}$ and P_e is between 0.12 and 0.3 dyn cm⁻² (Table 4). This corresponds to a relatively low density and low pressure. Assuming a temperature around 15 000 K, the microturbulence ξ is around 37.5 km s⁻¹, this is a relatively large but not really sensitive to the temperature, parameter that we have assumed. It is consistent with the results found by Heinzel et al. (1992).

7. Conclusion

We have presented a fast method of deriving physical parameters of post-flare loop spectra observed on the disk, principally the velocity field. It is a powerful method taking into account the bright background and getting 2 D maps of the parameters. We have applied this method to spectra scanning an active region overlaid by post-flare loops observed on May 16, 1981 with the SSHG spectrograph of Yunnan observatory. We have compared these results with the ones obtained with other methods and found a good agreement. Nevertheless the results found for the background cannot be used individually, they should be tested by a complete non-LTE transfer analysis.

Acknowledgements. One of us (X.M.Gu) highly appreciates the kind hospitality extended to him during his visit at Meudon Observatory, where the work was done. He expresses heartfelt thanks to the French Centre National de la Recherche (CNRS) and the Chinese National Science Foundation (CNSF) for financial supports. We are thankful to Drs P. Mein, N.Mein and P.Démoulin for their help and Dr. Heinzel for fruitful discussions. We will also thank Lin Jun for help in computer programme.

Appendix: mathematical method

In general, the intensity value of a spectral line at a point with wavelength λ_j can be written

$$I_{\lambda_j} = F(\lambda_j, \mathbf{X}), \quad (1)$$

where $\mathbf{X} = (x_1, x_2, \dots, x_{4m})$ and x_1, x_2, \dots, x_{4m} are 4m independent physical parameters (for the m-cloud model).

According to the least square method, the best representation of the total intensity $I_{\lambda_j}^{tol}$ observed is obtained when

$$\psi(\mathbf{X}) = \sum_{j=1}^n [F(\lambda_j, \mathbf{X}) - I_{\lambda_j}^{tol}]^2 \quad (2)$$

is a minimum. Here $I_{\lambda_j}^{tol}$ is the intensity observed at j^{th} wavelength point, n is the total number of wavelength points mea-

Table 4. Approximations of parameters derived with the ‘two/one-cloud model’ methods for the flare of May 16, 1981

Parameters	$N_{2,1}$	$N_{2,2}$	ξ_1	ξ_2	$n_{e,2}$	$P_{e,2}$
Profile						
No.	10^{13}cm^{-2}	10^{13}cm^{-2}	km s^{-1}	km s^{-1}	10^{10}cm^{-3}	dyn cm^{-2}
4757	0.535	0.166	41.716	23.680	2.306	0.121
4759	0.532	0.286	39.645	45.789	3.027	0.158
4760	0.767	0.196	44.941	45.188	2.506	0.131
4761	0.715	0.405	63.959	56.916	3.602	0.185
4762	0.752	0.579	67.541	41.593	4.307	0.227
4763	0.647	0.181	40.281	53.702	2.408	0.123
4765	0.433	0.464	50.886	30.688	3.855	0.202
4766	0.949	0.356	42.212	13.275	3.377	0.175
4768	0.272	0.429	49.355	27.130	3.707	0.193
4658	0.427		36.835			
4659	0.491		32.721			
4660	0.343	0.200	31.963	35.419	2.531	0.133
4661	0.262	0.256	34.531	35.850	2.864	0.149
4662	0.206	0.427	29.589	36.085	3.699	0.189
4663	0.122	0.588	24.876	34.146	4.340	0.220
4664	0.234	0.988	49.944	30.494	5.626	0.292
4665		0.592		26.712	4.355	0.225
4666		0.355		23.942	3.372	0.170
4667		0.254		23.244	2.853	0.130
4669		0.211		21.049	2.600	0.130

Subscript “1” indicates flare ribbons while subscript “2” indicates loops.

sured. The vector that minimizes $\psi(\mathbf{X})$ must satisfy the following equation

$$\frac{\partial\psi(\mathbf{X})}{\partial X_k} = 2 \sum_{j=1}^n [F_j(\lambda_j, \mathbf{X}) - I_{\lambda_j}^{tol}] \frac{\partial F_j}{\partial X_k} = 0, \quad (3)$$

where $F_j = F(\lambda_j, \mathbf{X})$. In general, Eq. (6) is non-linear and can be solved by using a complete linearization method. If we assume that \mathbf{X}_0 is an approximate solution and $\mathbf{X} = \mathbf{X}_0 + \delta\mathbf{X}$, we have

$$\phi_k(\mathbf{X}_0 + \delta\mathbf{X}) = \frac{\partial\psi(\mathbf{X}_0 + \delta\mathbf{X})}{\partial X_k} = 0. \quad (4)$$

Expanding $\phi_k(\mathbf{X}_0 + \delta\mathbf{X})$ into Taylor series in the neighbourhood of X_0 and neglecting the infinitesimal item of δX^2 and those after it, we obtain the linearized equation

$$\sum_{i=1}^{4m} \sum_{j=1}^n \{ [F_j(\mathbf{X}) - I_{\lambda_j}^{tol}] \times \frac{\partial^2 F_j}{\partial X_k \partial X_i} + \frac{\partial F_j}{\partial X_i} \frac{\partial F_j}{\partial X_k} \} \delta X_i + \phi_k(\mathbf{X}_0) = 0, \quad (5)$$

where $k=1, 2, \dots, 4m$, ($4m < n$). This equation which can be solved iteratively. and Eq. (8) can be expressed as

$$\mathbf{A} \bullet \delta\mathbf{X} = \mathbf{B}, \quad (6)$$

where \mathbf{A} is a $4m \times 4m$ matrix. Each element $A_{k,i}$ ($i, k = 1, 2, \dots, 4m$) is given by

$$A_{k,i} = 2 \sum_{j=1}^n \{ [F_j(\mathbf{X}) - I_{\lambda_j}^{tol}] \frac{\partial^2 F_j}{\partial X_k \partial X_i} + \frac{\partial F_j}{\partial X_i} \frac{\partial F_j}{\partial X_k} \}. \quad (7)$$

\mathbf{B} is a vector of $4m$ elements and each one is given by

$$B_k = -\phi_k(\mathbf{X}_0) \quad (8)$$

and $\delta\mathbf{X} = (\delta X_1, \delta X_2, \dots, \delta X_{4m})$. From Eq. (9), one can obtain

$$\delta\mathbf{X} = \mathbf{A}^{-1} \bullet \mathbf{B} \quad (9)$$

so, $\mathbf{X} = \mathbf{X}_0 + \delta\mathbf{X}$. We take the \mathbf{X} as \mathbf{X}_0 and substitute it into Eq. (12) and find a new $\delta\mathbf{X}$ in the same way and so on until the $\delta\mathbf{X} \rightarrow 0$. Because the convergence is proportional to $(\delta X/X)^2$, the convergence is quick.

Application of the method

$$I_{\lambda}^{tol} = S_1(1 - e^{-\tau_{\lambda,1}}) + S_2(1 - e^{-\tau_{\lambda,2}})e^{-\tau_{\lambda,1}} + S_3(1 - e^{-\tau_{\lambda,3}})e^{-(\tau_{\lambda,1} + \tau_{\lambda,2})} \quad (10)$$

We take the $I_{\lambda}^{tol} = F(\lambda, \mathbf{X})$, where $\mathbf{X} = (x_1, x_2, \dots, x_{12})$ and x_1, x_2, \dots, x_{12} correspond to the four physical parameters of three subloops (indicated by subscript 1, 2 and 3), respectively.

References

- Beckers, J.M., 1964, *Ph.D.Thesis*, Utrecht
 Cheng, C.C., 1980, *Solar Phys.*, 65, 347
 Fang, C., 1985, *Publications of Nanjing University*, 21, 301
 Feldman, U. and Seely, J.F., 1995, *ApJ*, 450, 902
 Forbes, T.G. and Malherbe J.M., 1986, *ApJ*, 302, L67
 Forbes T.G. and Acton, L., 1996, *ApJ*, 459, 330
 Gu, X.M., Lin, J., Luan, T., Schmieder, B., 1992, *A&A*, 259, 649
 Heinzel, P, Schmieder, B, Mein, P., 1992, *Solar Phys.*, 139, 81

- Heinzl, P., Gouttebroze, P., Vial, J.C., 1994, *A&A*, 292, 656
- Luo, Z., 1987, *MSc Thesis*, Yunnan Observatory
- Masuda, S., Kosugi, T., Hara, H., Tsuneta, S., 1994, *Nature*, 371, 495
- Mein, P. and Mein, N., 1989, *A&A*, 203, 162
- Mein, N., Mein, P., Heinzl, P. et al., 1996, *A&A*, 309, 275
- Poland, A., Skumanich, A., Athay, R.G., Tandberg-Hanssen, E., 1971, *Solar Phys.*, 18, 391
- Schmieder, B., Švestka, Z., Jackson, V. and Machado, M.E. (eds), 1992, *Lecture Notes in Physics*, 399, 124
- Schmieder, B., Forbes, T.G., Malherbe, J.M. and Machado, M.E., 1987, *ApJ*, 317, 956
- Schmieder, B., Malherbe, J.M., Simnett, G.M., Forbes, T.G., Tandberg-Hanssen E., 1990, *ApJ*, 356, 720
- Schmieder, B., Heinzl, P., Wiik, J.E. et al., 1995, *Solar Phys.*, 156, 337
- Schmieder, B., Heinzl, P., van-Driel-Gesztelyi, L and Lemen, J.R., 1996, *Solar Phys.*, 165, 303
- Švestka, Z., 1989, *Solar Phys.*, 121, 399
- Švestka, Z., Fontenla, J.M., Machado, M.E., et al., 1987, *Solar Phys.*, 108, 237
- Tsuneta, S., 1996a, *Solar and Astrophysical Magnetohydrodynamic Flows*, ed. K.C. Tsinganos, Kluwer, 85
- Tsuneta, S., 1996b, *ApJ*, 464, 1055
- Wiik, J.E., Schmieder, B., Heinzl, P., Roudier, T., 1996, *Solar Phys.*, 166, 89